Free Vibrational Characteristics of Sandwich Cylindrical Shells Containing a Zero Poisson's Ratio Cellular Core

Leipeng Song[1] · Taoxi Wang[1] · Zhiyong Yin[2] · Xing Shen[1] · Hongjie Wang[1] · Chao Yin[1]

Abstract

Purpose Cellular configurations with ZPR more suitable for cylindrical sandwich shell in which the structure needs undergo pure cylindrical bending. To date, research in the vibration response of cylindrical sandwich shell is still a challenging task. This article proposes one method for free vibration analysis of sandwich cylindrical shells consisting of elastic-isotropic skin and a zero Poisson's ratio cellular core was proposed.

Method The free vibration characteristics of the sandwich cylindrical shells has been studied using classical thin shell theory. Theoretical models of the effective mechanical performances of the cellular core are established by homogenization methods. The accuracies of theoretical predictions are validated by the finite element method and comparing with others from some available literatures.

Results and Conclusions Based on the theoretical predictions, the influences on effective mechanical performances of the cellular core and natural frequencies of the sandwich cylindrical shell caused by geometric parameters are evaluated in detail. These geometrical parameters provide different contributions to the effective mechanical properties and dynamic response, which can lead to separate designs for improving their dynamic characteristics.

Keywords Sandwich cylindrical shells · ZPR · Mechanical performances · Vibrational behaviors · Theoretical prediction

Introduction

As an advanced material and structure, the cellular structure has shown great potential for automotive, aerospace, and marine applications due to its outstanding properties, including high strength-to-weight ratio and specific stiffness, as well as good structural stability and energy absorption [1–3]. Shell structures are one of the most important structures in engineering applications. Sandwich cylindrical shells with cellular core not only remain the characteristics of cellular structure but also embody the special geometry, resulting in sandwich cylindrical shells have been shown great potential in a wide range of gas and fluid storage tanks, solar cell shells, flexible pipe, etc. [4, 5]. These structures are always

suffering from dynamic loads at their service. Therefore, vibration characteristics analysis of sandwich cylindrical shells with cellular core has become extremely important.

Cellular structures are generally considered homogeneous orthotropic materials by predicting their equivalent properties, regardless of the complexity of the internal structures [6]. Up to now, researchers have been working extensively on the various calculated methods of effective elastic properties of cellular structures, among the common methods are energy [7, 8] and homogenization methods [9, 10]. Gibson explores the effective mechanical properties of hexagonal honeycomb based on the energy method [11]. However, Gibson's model showed some errors in the theoretical results due to the neglect of the axial deformation and shear deformation, resulting that some research focusing on the revision of Gibson's theory [12]. In addition, traditional hexagonal honeycombs with positive Poisson's ratio (PPR) can no longer keep up with the growing demand for capricious practical applications. Numerous novel structures have been developed and applied with the characteristic of negative Poisson's ratio (NPR) [13, 14], zero Poisson's ratio (ZPR) [15, 16], and tailorable Poisson's ratio [17] in recent years.

✉ Zhiyong Yin
  cssrc702yzy@163.com

1 State Key Laboratory of Mechanics and Control of Mechanical Structures, Nanjing University of Aeronautics and Astronautics, Nanjing 210016, China

2 National Key Laboratory of Ship Vibration & Noise, China Ship Science Research Center, Wuxi 214082, China

However, when subjected to pure bending, the NPR cellular structures exhibit a saddle-like curvature, while the PPR cellular structures exhibit a dome-like curvature [18], which makes the processing of sandwich cylindrical shells with cellular core considerably more complicated and precludes their application on some special occasions. Zero Poisson's ratio (ZPR) feature can preclude a significant increase of effective stiffness in the horizontal direction by limiting the contraction (or bulging) in the vertical direction [19, 20].

Up to now, there are three typical theories to predict the vibrational behavior of composite cylindrical plates/shells: (1) the classical laminate plates/shells theory (CLPT/CLST), (2) the First-order shear deformation theory (FSDT), and (3) the High-order shear deformation theory (HSDT). Reissner modified the CLPT and proposed the FSDT by considering the effect of shear deformation [21]. Reddy developed an HSDT of laminated composite plates [22]. Wang et al. [23] derived the nonlinear equations for laminated composite structures. Duc et al. [24] discussed the nonlinear response of functionally graded (FG) cylindrical shells based on the Donnell classical shell theory by applying the Galerkin's method. Qin et al. [25] utilized the FSDT to present the free vibration of rotating FG carbon nanotube-reinforced composite cylindrical shells. Pang et al. [26] extracted the displacement functions of combined composite laminated cylindrical and spherical shells using the FSDT. Eipakchi et al. [27] studied the vibrational behavior of an auxetic composite cylindrical shell based on the CLST and Hamilton's principle.

As is reviewed from the published literatures, many researchers have been working extensively on the equivalent mechanical performances of cellular core and vibration issues of composite structures. However, a limited number of research articles are available to study the vibration behavior of sandwich cylindrical shells with ZPR honeycomb core. No saddle-like or dome-like curvature could be found for structure exhibiting ZPR under out-of-plane bending, which makes ZPR cellular configurations more suitable for cylindrical sandwich shell in which the structure needs undergo pure cylindrical bending. Therefore, it is more advantageous in terms of structural stability compared to other honeycomb structures and is more suitable to be incorporated in the design of piping structures.

Summarizing, the originality of the present paper lies in exploring the free flexural vibration characteristics of sandwich cylindrical shells containing a ZPR cellular core in the light of equivalent single-layer theory. The main contents are as follows: First, the effective mechanical performances of the ZPR cellular core are deduced in detail. Second, the Hamilton principle and CLST are utilized to establish the governing equations and mathematical model. Thirdly, FEM and some available literature results are introduced to prove the feasibility and correctness of the current method. Last, parametric analysis shows the influences of structural parameters on the mechanical performances of the cellular core and the free vibrational behavior of sandwich cylindrical shells.

Formulations

Figure 1 shows the schematic sketch and the coordinate system of the sandwich cylindrical shell containing the ZPR cellular core layer, where the radius of middle surface is R, the thickness is h, and the length is L. The cylindrical shell is composed of three layers, the inner layer and outer layer are elastic and isotropic materials with equal thickness, and the middle layer is a cellular structure with a thickness of h_0. In addition, an orthogonal coordinate system (z, x, and θ) is fixed at the middle surface. The deformations of the point at the shell's middle surface are denoted U_x, U_θ, and U_z, in the x, θ, and z directions, respectively. A coordinate (z_k, $k = 1,2,3,4$) is defined for each layer as shown in Fig. 1, in which $Z_1 = \frac{h}{2}$, $Z_2 = \frac{h_0}{2}$, $Z_3 = -\frac{h_0}{2}$, and $Z_4 = -\frac{h}{2}$.

Effective Mechanical Performances of Cellular Core Layer with ZPR

When analyzing the vibrational behavior of the sandwich cylindrical shell containing the ZPR cellular core, we first need to predict the effective mechanical performances of the

Fig. 1 Schematic sketch and the coordinate system of the sandwich cylindrical shell
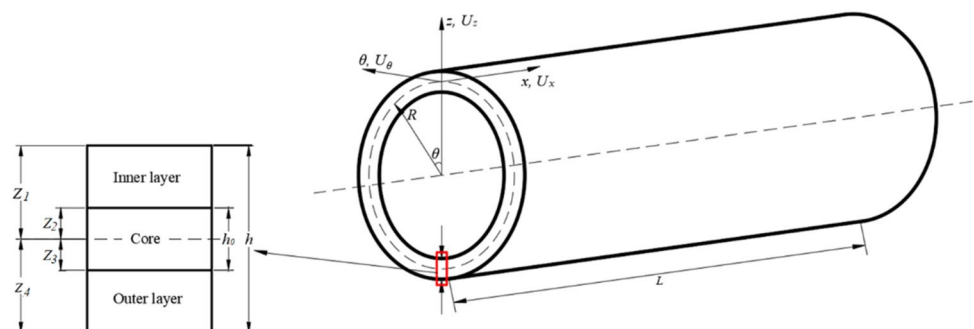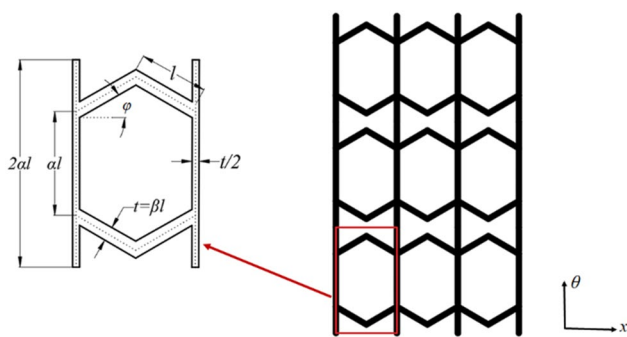
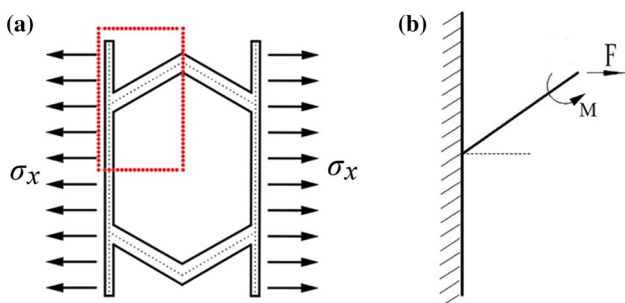**Fig. 2** Geometrical parameters of the ZPR cellular core

Fig. 3 Schematic illustration of unit cell model used to calculate the elastic modulus in direction-*x*: **a** tensile stress along direction-*x*; **b** simplified model

ZPR cellular core. There are several assumptions made for the theoretical analysis:

(1) The formulation is based on the Euler–Bernoulli beam theory;
(2) All the joints of the cellular walls are considered to be rigid.

Figure 2 illustrates the schematic diagram of the ZPR cellular, where φ is internal angles, l represents the length of diagonal walls, $2\alpha l$ represents the length of vertical walls, and $t = \beta l$ represents the thickness of sloping walls. Here, α and β represent the aspect and cell wall thickness ratios, respectively.

Unit cell structure is selected and illustrated in Fig. 3(a). The first step for the unit cell model is a simplification, as shown in Fig. 3(b), which transforms the model into a quarter model owing to the biaxial symmetry. After simplification, a fixed boundary is set to the left end of the model, while the right is set with a concentrated force F and a moment M. On the one hand, the deformation of the ZPR cellular structure is driven mainly by the sloping walls' bending deformation when honeycombs withstand a load along direction-*x* [28]. On the other hand, the vertical wall length along direction-*x* is smaller than that of

the sloping walls. Therefore, the tensile deformation of the vertical walls is ignored, only the bending and tensile deformation of the sloping walls are considered.

According to the equilibrium equations [29], it can be concluded that the vertical force is zero, and the moment M is:

$$M = \frac{1}{2} Fl \sin \varphi \tag{1}$$

The strain energy U of a cantilever beam subjected to bending moment $M(x)$ and axial load $F_N(x)$ can be expressed as:

$$U = \int_0^l \frac{M^2(x)}{2EI} dx + \int_0^l \frac{F_N^2(x)}{2EA} dx \tag{2}$$

where E, I, and A are the elastic modulus, inertia moment, and cross-sectional area, respectively.

In this paper, it is assumed that the bending moment in the anti-clockwise direction is positive. By now, the bending moment is:

$$M(x) = \left(\frac{1}{2} l - x \right) F \sin \varphi \tag{3}$$

And the axial load is:

$$F_N(x) = F \cos \varphi \tag{4}$$

Combining Eqs. (2), (3), and (4), it can be concluded that the strain energy U is:

$$U = \frac{F^2 l^3 \sin^2 \varphi}{24 E_s^c I} + \frac{F^2 l \cos^2 \varphi}{2 E_s^c A} \tag{5}$$

where E_s^c is the elastic modulus of raw materials.

According to Castigliano's second theorem [30], when the elastic system is enduring static load, the displacement δ_i of the point of force action can be calculated by the partial derivative of the strain energy U for any applied force F_i:

$$\delta_i = \frac{\partial U}{\partial F_i} \tag{6}$$

Combining Eqs. (5) and (6), it can be concluded that horizontal displacement of the point of force action is:

$$\delta_x = \frac{Fl^3 \sin^2 \varphi}{12 E_s^c I} + \frac{Fl \cos^2 \varphi}{E_s^c A} \tag{7}$$

According to the homogenization theory [31], the equivalent tensile modulus in direction-*x* can be deduced:

$$\sigma_x = \frac{F}{\alpha l h_0} \tag{8}$$

$$\varepsilon_x = \frac{\delta_x}{l \cos \varphi} \tag{9}$$

$$E_x = \frac{\sigma_x}{\varepsilon_x} \tag{10}$$

where σ_x and ε_x are the equivalent stress and strain in direction-x, respectively.

Substituting Eqs. (7), (8) (9) into Eq. (10), it can be concluded that the equivalent elastic modulus in direction-x can be expressed as:

$$E_x = E_s^c \frac{\beta^3 \cos \varphi}{\alpha (\sin^2 \varphi + \beta^2 \cos^2 \varphi)} \tag{11}$$

Similarly, Fig. 4 shows the schematic illustration of the unit cell model used to calculate the elastic modulus in direction-θ.

In this case, the strain energy U is:

$$U = \frac{F^2 \alpha l}{E_s^c A} \tag{12}$$

Then, displacement in direction-θ of the point of force action is:

$$\delta_\theta = \frac{2F\alpha}{E_s^c \beta h_0} \tag{13}$$

According to the homogenization theory, the equivalent tensile modulus along direction-x can be deduced:

$$\sigma_\theta = \frac{F}{h_0 l \cos \varphi} \tag{14}$$

$$\varepsilon_\theta = \frac{\delta_\theta}{2\alpha l} \tag{15}$$

$$E_\theta = \frac{\sigma_\theta}{\varepsilon_\theta} \tag{16}$$

where σ_θ and ε_θ are the equivalent stress and strain in direction-θ, respectively

Substituting Eqs. (13), (14), (15) into Eq. (16), it can be concluded that the equivalent tensile modulus along direction-θ can be expressed as:

$$E_\theta = E_s^c \frac{\beta}{\cos \varphi} \tag{17}$$

The rotation of the joints in the structure is assumed to be zero owing to the structural symmetry. According to the above assumptions, it is considered that the deformations of sloping walls and vertical walls have relative independence, resulting that the strain along direction-x being zero when the cellular structure suffers a tensile loading along the direction-θ. Likewise, the above consideration also applies to the deformation of cellular structure along direction-x. Therefore, both values of the Poisson's ratio $\mu_{\theta x}$ and $\mu_{x\theta}$ are considered to be zero.

The relative density of the ZPR cellular core is

$$\rho = \rho^c \frac{(2 + \alpha)\beta}{2\alpha \cos \varphi} \tag{18}$$

where ρ^c is the density of raw materials.

Vibrational Behavior of the Cylindrical Shell

Governing Equations

The assumptions generally employed in Sect. "Vibrational Behavior of the Cylindrical Shell" are:

(1) The sandwich cylindrical shells are thin shells, and the shell thickness is less than 10% of the shell radius.
(2) No external load is borne to the sandwich cylindrical shell.
(3) Compared with the radius of the sandwich cylindrical shell, its deformations are small. The cross-section of the sandwich cylindrical shell remains perpendicular to the middle surface after deformation.
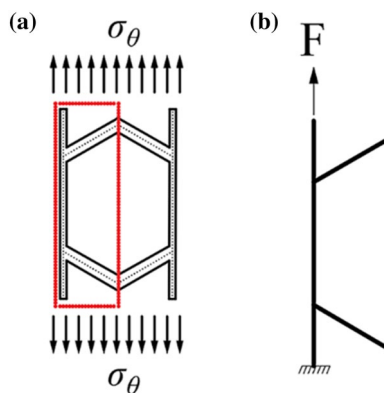(4) Rotary inertia and shear deformation are neglected.

Fig. 4 Schematic illustration of unit cell model used to calculate the elastic modulus in direction-θ: **a** tensile stress along direction-θ; **b** simplified model

(5) The outer and inner layers are bonded perfectly to the middle layer.

Duo to axisymmetry, arbitrary particle displacement of the cylinder caused by bending, based on the CLST [32] is:

$$\begin{cases} U_x(x,z,t) = u(x,t) - z\dfrac{\partial w(x,t)}{\partial x} \\ U_\theta(x,z,t) = 0 \\ U_z(x,z,t) = w(x,t) \end{cases} \tag{19}$$

According to the linear kinematic relations [33], strain–displacement relations are:

$$\begin{cases} \varepsilon_x = \dfrac{\partial U_x}{\partial x} = \dfrac{\partial u}{\partial x} - z\dfrac{\partial^2 w}{\partial x^2} \\ \varepsilon_\theta = \dfrac{U_z}{r} = \dfrac{w}{R+z} \end{cases} \tag{20}$$

Based on Hooke's law [34], the stress–strain relations of the thin sandwich cylindrical shell are as the following:

$$\begin{Bmatrix} \sigma_x \\ \sigma_\theta \end{Bmatrix} = \begin{pmatrix} Q_{11}^{(k)} & Q_{12}^{(k)} \\ Q_{21}^{(k)} & Q_{22}^{(k)} \end{pmatrix} \begin{Bmatrix} \varepsilon_x \\ \varepsilon_\theta \end{Bmatrix}, k = 1, 2, 3 \tag{21}$$

where $Q_{ij}^{(k)}(i, j = 1, 2)$ are elastic constants and given as

$$\begin{cases} Q_{11}^{(k)} = E_x^{(k)} / \left(1 - \mu_{x\theta}^{(k)}\mu_{\theta x}^{(k)}\right) \\ Q_{12}^{(k)} = E_\theta^{(k)}\mu_{x\theta}^{(k)} / \left(1 - \mu_{x\theta}^{(k)}\mu_{\theta x}^{(k)}\right) \\ Q_{21}^{(k)} = E_x^{(k)}\mu_{\theta x}^{(k)} / \left(1 - \mu_{x\theta}^{(k)}\mu_{\theta x}^{(k)}\right) \\ Q_{22}^{(k)} = E_\theta^{(k)} / \left(1 - \mu_{x\theta}^{(k)}\mu_{\theta x}^{(k)}\right) \end{cases}, k = 1, 2, 3 \tag{22}$$

where $E_x^{(k)}$ and $E_\theta^{(k)}$ are effective elastic modulus of the inner, outer, and core layer. $\mu_{\theta x}^{(k)}$ and $\mu_{x\theta}^{(k)}$ are the Poisson's ratios. $k = 1$, 2, and 3 stand for the inner, core, and outer layers, respectively.

For simplicity, it is assumed that the inner and outer layers have the same material performances with elastic modulus E, density ρ^t, and Poisson's ratio μ. Therefore, we obtain:

$$\begin{cases} E_x^{(1)} = E_x^{(3)} = E_\theta^{(1)} = E_\theta^{(3)} = E \\ \mu_{x\theta}^{(1)} = \mu_{x\theta}^{(3)} = \mu_{\theta x}^{(1)} = \mu_{\theta x}^{(3)} = \mu \\ \rho^{(1)} = \rho^{(3)} = \rho^t \end{cases} \tag{23}$$

The equivalent material performances of the ZPR cellular, including elastic modulus, density, and Poisson's ratios, are obtained in Sect. "Effective Mechanical Performances of Cellular Core Layer with ZPR":

$$\begin{cases} E_x^{(2)} = E_s^c \dfrac{\beta^3 \cos\varphi}{\alpha(\sin^2\varphi + \beta^2\cos^2\varphi)} \\ E_\theta^{(2)} = E_s^c \dfrac{\beta}{2\cos\varphi} \\ \mu_{x\theta}^{(2)} = \mu_{\theta x}^{(2)} = 0 \\ \rho^{(2)} = \rho^c \dfrac{(2+\alpha)\beta}{2\alpha\cos\varphi} \end{cases} \tag{24}$$

The kinetic energy T, strain energy U and the external work W, are given as:

$$\tag{25}$$

$$\begin{cases} T = \dfrac{1}{2}\left\{ \sum_{k=1}^{3}\left[\int_0^t \int_{z_k}^{z_{k+1}} \int_0^l \int_0^{2\pi} \rho^{(k)}\left(\left(\dfrac{\partial U_x}{\partial t}\right)^2 + \left(\dfrac{\partial U_z}{\partial t}\right)^2 \right)(R+z)d\theta dx dz dt \right] \right\} \\ U = \dfrac{1}{2}\left\{ \sum_{k=1}^{3}\left[\int_0^t \int_{z_k}^{z_{k+1}} \int_0^l \int_0^{2\pi} \left(\sigma_x^{(k)}\varepsilon_x^{(k)} + \sigma_\theta^{(k)}\varepsilon_\theta^{(k)} \right)(R+z)d\theta dx dz dt \right] \right\} \\ W = 0 \end{cases}$$

The governing equations of the sandwich cylindrical shell containing the ZPR cellular core are based on deduction from Hamilton's principle [35]:

$$\begin{cases} R\dfrac{\partial N_x}{\partial x} - C_2\dfrac{\partial^2 u}{\partial t^2} - \dfrac{C_3}{2}\dfrac{\partial^3 w}{\partial x\partial t^2} = 0 \\ C_1\dfrac{\partial^4 w}{\partial x^2\partial t^2} - C_2\dfrac{\partial^2 w}{\partial t^2} + \dfrac{C_3}{2}\dfrac{\partial^3 u}{\partial x\partial t^2} + R\dfrac{\partial^2 M_x}{\partial x^2} - N_\theta = 0 \end{cases} \tag{26}$$

where

Table 1 Value of α_i, η and λ_m for different boundary conditions [37]

Boundary conditions	α_i	η	λ_m
SS-SS	$\alpha_1 = 0, \alpha_2 = 0,$ $\alpha_3 = 0, \alpha_4 = -1,$	$m\pi$	1
F-SS	$\alpha_1 = 1, \alpha_2 = 1,$ $\alpha_3 = 1, \alpha_4 = 1,$	$\tan\eta = \tanh\eta$	$\frac{\cosh\eta - \cos\eta}{\sinh\eta - \sin\eta}$
C-SS	$\alpha_1 = 1, \alpha_2 = -1,$ $\alpha_3 = 1, \alpha_4 = -1,$	$\tan\eta = \tanh\eta$	$\frac{\cosh\eta - \cos\eta}{\sinh\eta - \sin\eta}$

Table 2 Boundary conditions on FE models to calculate the mechanical properties of cellular core

	Moduli along direction-x	Moduli along direction-θ
Boundary A	$u_x = u_\theta = u_z$	free
Boundary B	$u_x = $ imposed, $u_\theta = u_z = 0$	free
Node C	Free	$u_x = u_\theta = u_z$
Node D	Free	$u_x = u_\theta = u_z$
Node E	Free	$u_\theta = $ imposed, $u_x = u_z = 0$
Node F	Free	$u_\theta = $ imposed, $u_x = u_z = 0$

Table 3 Material performances of cellular core in FEM

	Properties (unit)	Quantity
Material performances of cellular core	α	2
	β	0.1
	$E_s^c (GPa)$	200
	Poisson's ratio	0.3
	$\rho^c \ (kg/m^3)$	7800
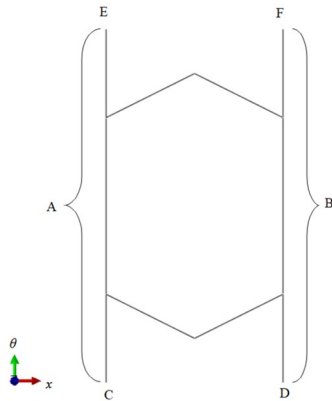
Fig. 5 The 2D geometric model for the simulation of the mechanical properties of cellular core
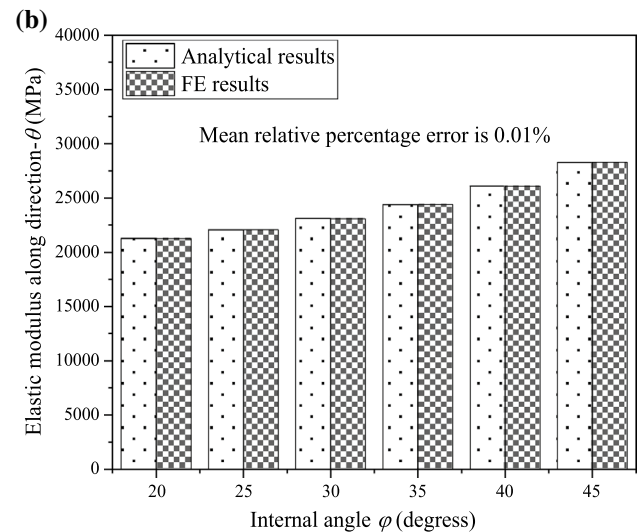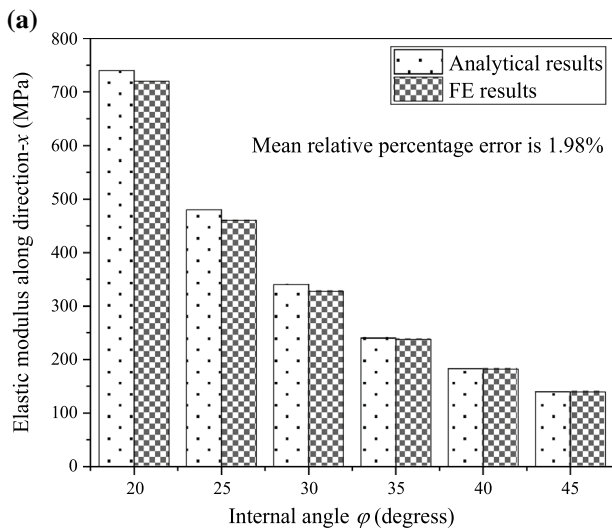
Fig. 6 Theoretical and simulation results of effective mechanical properties of cellular core: **a** effective elastic modulus in direction-x, **b** effective elastic modulus in direction-θ

$$\begin{cases} -2R\left(N_x \delta u\right)\Big|_{x=0}^{x=L} = 0 \Rightarrow N_x = 0 \; OR \; u = 0 \; at \; x = 0, L \\[2mm] \left(-2C_1\dfrac{\partial^3 w}{\partial x \partial t^2} - C_3\dfrac{\partial^2 u}{\partial t^2} - 2R\dfrac{\partial M_x}{\partial x}\right)\delta w\Big|_{x=0}^{x=L} = 0 \Rightarrow -2C_1\dfrac{\partial^3 w}{\partial x \partial t^2} - C_3\dfrac{\partial^2 u}{\partial t^2} - 2R\dfrac{\partial M_x}{\partial x} = 0 \; OR \; w = 0 \; at \; x = 0, L \\[2mm] \left(2RM_x\delta\left(\dfrac{\partial w}{\partial x}\right)\right)\Big|_{x=0}^{x=L} = 0 \Rightarrow M_x = 0 \; OR \; \dfrac{\partial w}{\partial x} = 0 \; at \; x = 0, L \end{cases} \tag{30}$$

$$\begin{cases} N_x = \displaystyle\sum_{k=1}^{3} \int_{z_k}^{z_{k+1}} \sigma_x^{(k)} \dfrac{R+z}{R} dz \\[3mm] M_x = \displaystyle\sum_{k=1}^{3} \int_{z_k}^{z_{k+1}} \sigma_x^{(k)} \dfrac{R+z}{R} z\, dz \\[3mm] N_\theta = \displaystyle\sum_{k=1}^{3} \int_{z_{k-1}}^{z_k} \sigma_\theta^{(k)} dz \\[3mm] C_1 = \dfrac{1}{12}\rho^t R(h^3 - h_0^3) + \dfrac{1}{12}\rho^{(2)} R h_0^3 \\[2mm] C_2 = \left[\rho^t(h - h_0) + \rho^{(2)} h_0\right] R \\[2mm] C_3 = -\dfrac{1}{6}\rho^{(2)} h_0^3 - \dfrac{1}{6}\rho^t\left(h^3 - h_0^3\right) \end{cases} \tag{27}$$

Then, the governing equations rewrite as follows:

$$\begin{cases} A_{11}\dfrac{\partial^3 w}{\partial x^3} - A_{12}\dfrac{\partial^2 u}{\partial x^2} - A_{13}\dfrac{\partial w}{\partial x} - \dfrac{C_3}{2}\dfrac{\partial^3 w}{\partial x \partial t^2} - C_2\dfrac{\partial^2 u}{\partial t^2} = 0 \\[3mm] C_1\dfrac{\partial^4 w}{\partial x^2 \partial t^2} + A_{21}\dfrac{\partial^4 w}{\partial x^4} - C_2\dfrac{\partial^2 w}{\partial t^2} + \dfrac{C_3}{2}\dfrac{\partial^3 u}{\partial x \partial t^2} \\[3mm] \quad - A_{22}\dfrac{\partial^3 u}{\partial x^3} + A_{23}\dfrac{\partial u}{\partial x} + A_{24} w = 0 \end{cases} \tag{28}$$

where

$$\begin{cases} A_{11} = A_{22} = \dfrac{E\left(h^3 - h_0^3\right)}{12\left(\mu^2 - 1\right)} - \dfrac{E_x^{(2)} h_0^3}{12} \\[3mm] A_{12} = \dfrac{ER(h - h_0)}{\mu^2 - 1} - E_x^{(2)} R h_0 \\[3mm] A_{13} = A_{23} = \dfrac{E\mu}{\left(\mu^2 - 1\right)}\left(h - h_0\right) \\[3mm] A_{21} = \dfrac{ER(h^3 - h_0^3)}{12\left(\mu^2 - 1\right)} - \dfrac{E_x^{(2)} R h_0^3}{12} \\[3mm] A_{24} = \dfrac{1}{12}\dfrac{E}{\mu^2 - 1}\left(h^3 - h_0^3\right)\dfrac{1}{R^3} - \dfrac{1}{12}E_\theta^{(2)} h_0^3 \dfrac{1}{R^3} \\[3mm] \quad + \dfrac{E}{\mu^2 - 1}\left(h - h_0\right)\dfrac{1}{R} - E_\theta^{(2)} h_0 \dfrac{1}{R} \end{cases} \tag{29}$$

According to Hamilton's principle, the boundary conditions are also given as:

Boundary conditions may be written as:

$$w = N_x = M_x = 0 \tag{31a}$$

simply supported boundary (SS)

$$u = w = \dfrac{\partial w}{\partial x} = 0 \tag{31b}$$

clamped supported boundary (C)

$$N_x = M_x = -2C_1\dfrac{\partial^3 w}{\partial x \partial t^2} - C_3\dfrac{\partial^2 u}{\partial t^2} - 2R\dfrac{\partial M_x}{\partial x} = 0 \tag{31c}$$

free boundary (F)

Natural Frequency

For a cylindrical shell with different boundaries, as shown in Fig. 1, one can assume the solution forms of the field of spatial displacement as [36]:

$$\begin{cases} u = A\dfrac{\partial \phi(x)}{\partial x}\sin(\omega t) \\[3mm] w = B\phi(x)\sin(\omega t) \end{cases} \tag{32}$$

where A and B are two unknown coefficients, and ω denotes the angular frequency.

By substituting Eqs. (32) into Eqs. (31a, 31b, 31c), boundary conditions then become:

$$\begin{cases} \phi(x) = \dfrac{\partial^2 \phi(x)}{\partial x^2} = 0, (SS) \\[3mm] \phi(x) = \dfrac{\partial \phi(x)}{\partial x} = 0, (C) \\[3mm] \dfrac{\partial^2 \phi(x)}{\partial x^2} = \dfrac{\partial^3 \phi(x)}{\partial x^3} = 0, (F) \end{cases} \tag{33}$$

The axial modal function $\phi(x)$ is defined as [37]:

Table 4 Natural frequencies of the isotropic elastic cylindrical shell under SS-SS boundary

Experiment [39, 40]	(SST Exact) [40]	SST (APP.) [40]	FST (Exact) [40]	FST (App.) [40]	MKST (Exact) [40]	MKST (APP.) [39]	DST (Exact) [40]	DST (APP.) [40]	FEM	Current method
138HZ	139HZ	141HZ	140HZ	142HZ	134HZ	142HZ	101HZ	149HZ	140HZ	145HZ

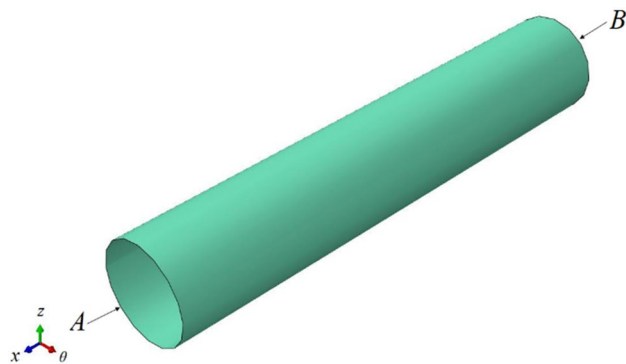**Fig. 7** 3D model for the simulation of the natural frequencies

$$\phi(x) = \alpha_1 \cosh\left(\frac{\eta x}{L}\right) + \alpha_2 \cos\left(\frac{\eta x}{L}\right) \\ - \lambda_m\left(\alpha_3 \sinh\left(\frac{\eta x}{L}\right) + \alpha_4 \sin\left(\frac{\eta x}{L}\right)\right) \tag{34}$$

where α_i ($i = 1,2,3,4$) values 0 or ± 1 are determined for each boundary condition. η is a natural number of axial waves. λ_m is a coefficient dependent on η. Table 1 shows the value of α_i, η and λ_m for different boundary conditions.

Substituting Eqs. (32), (33), and (34) into (28) results in a set of governing eigenvalue equations:

$$\begin{pmatrix} L_{11} & L_{12} \\ L_{21} & L_{22} \end{pmatrix} \begin{pmatrix} A \\ B \end{pmatrix} = \begin{pmatrix} 0 \\ 0 \end{pmatrix} \tag{35}$$

where

$$\begin{cases} L_{11} = C_2 \dfrac{\partial \phi}{\partial x}\omega^2 - A_{12}\dfrac{\partial^3 \phi}{\partial x^3} \\ L_{12} = A_{11}\dfrac{\partial^3 \phi}{\partial x^3} - A_{13}\dfrac{\partial \phi}{\partial x} + \dfrac{C_3}{2}\dfrac{\partial \phi}{\partial x}\omega^2 \\ L_{21} = A_{23}\dfrac{\partial^2 \phi}{\partial x^2} - \dfrac{C_3}{2}\dfrac{\partial^2 \phi}{\partial x^2}\omega^2 - A_{22}\dfrac{\partial^4 \phi}{\partial x^4} \\ L_{22} = A_{21}\dfrac{\partial^4 \phi}{\partial x^4} - C_1\dfrac{\partial^2 \phi}{\partial x^2}\omega^2 + C_2\phi\omega^2 + A_{24}\phi \end{cases} \tag{36}$$

To obtain the angular frequencies of the sandwich cylindrical shell, we solve the equation $\left|L_{ij}\right| = 0$. Then the following polynomial can be factorized into:

$$\lambda_1\omega^4 + \lambda_2\omega^2 + \lambda_3 = 0 \tag{37}$$

where, λ_i ($i = 1, 2, 3$) are constants. By solving Eq. (37), one can obtain two angular frequencies in the axial and radial directions. This investigation considers only the smallest angular frequency.

Table 5 Boundary conditions on FE models to calculate the natural frequencies

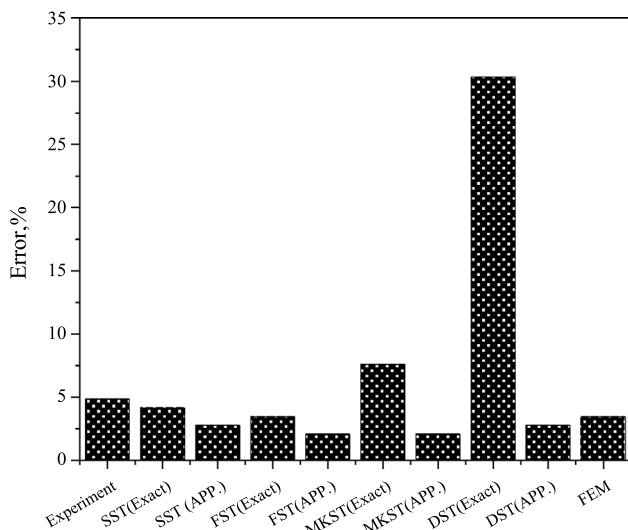|	SS-SS	SS-F	SS-C
A	$u_\theta = u_z = 0, UR_\theta = UR_z = 0$	$u_\theta = u_z = 0, UR_\theta = UR_z = 0$	$u_\theta = u_z = 0, UR_\theta = UR_z = 0$
B	$u_\theta = u_z = 0, UR_\theta = UR_z = 0$	free	$u_x = u_\theta = u_z = 0, UR_x = UR_\theta = UR_z = 0$

Fig. 8 Error for the natural frequencies of the SS-SS shell

Table 6 Geometry dimensions and material properties of sandwich cylindrical shells

	Properties (unit)	Quantity
Geometric dimension of the shell	L (m)	1
	R (m)	0.2
	h (mm)	10
	h_0 (mm)	8
Material properties of cellular core	α	2
	β	0.1
	φ (degree)	30
	E_s^c (GPa)	200
	Poisson's ratio	0.3
	Mass density (kg/m^3)	7800
Material properties of inner/outer layer	E (GPa)	0.008
	μ	0.3
	ρ^t (kg/m^3)	0.93

Numerical Simulation

In order to verify the calculation results in the above theories, numerical simulation with a commercial FE software ABAQUS (version 6.14) is carried out. Unit cell with a 2-node linear element B21 is used to analyze the effective mechanical performances of the ZPR cellular core, as shown

in Fig. 5. The tensile of the honeycomb under a linear static loading was developed by imposing concentrated force P along direction-x and direction-θ. The boundary conditions are listed in Table 2. The effective stress σ_{FEM} is calculated by $\sigma_{FEM} = \frac{P}{\alpha l h_0}$, The effective strain ε_{FEM} is calculated by $\sigma_{FEM} = \frac{P}{\alpha l h_0}$ and $\varepsilon_{FEM} = \frac{U_i}{2l\cos\varphi}$ ($i = 1, 2$), where U_1 and U_2 are the displacement along direction-x and direction-θ, respectively. The modulus along direction-x and direction-θ were then obtained as the ratios between the effective stresses and strains. Table 3 itemizes the corresponding material performances of the cellular core in FEM. The relative percentage error is given as:

$$Error(\%) = \frac{|\omega_{theoretical} - \omega_{FEM}|}{\omega_{theoretical}} \times 100\% \tag{38}$$

where $\omega_{theoretical}$ and ω_{FEM} are the theoretical and simulation results, respectively.

Figure 6 shows the theoretical and FE results of equivalent mechanical performances of the cellular core under different internal angles. One can see that the theoretical predictions of the elastic modulus of the cellular core are consistent with the simulation results both in direction-x and direction-θ. The mean relative percentage error of the elastic modulus in direction-x is 1.98%, while in direction-θ is 0.01%. The main reason is that the deformations of the vertical cellular walls are ignored in predicting the elastic moduli in direction-x. The simulation results, it should be noted, are somewhat below the theoretical ones, contributing to the difference between the simulation model and the theoretical model [38]. In fact, the beam model applied to the Finite element simulation is the Timoshenko beam, while to theoretical analysis is the Euler–Bernoulli beam. In addition, with the increase of the internal angle, the elastic moduli in direction-x decrease, while the elastic moduli in direction-θ grow.

To evaluate the accuracy of natural frequencies in the current method, Table 4 lists the natural frequencies of the isotropic elastic cylindrical shell under the SS-SS boundary calculated by the current method, FEM, experiment [39], and four shell theories [40]: (1) Soedel (SST), (2) Flügge (FST), (3) Morley-Koiter (MKST) and (4) Donnell (DST), where Exact and APP. denote exact and approximate solutions, respectively. If we chose $h_0 = 0$, the vibration characteristics of the sandwich cylindrical shell would turn into the
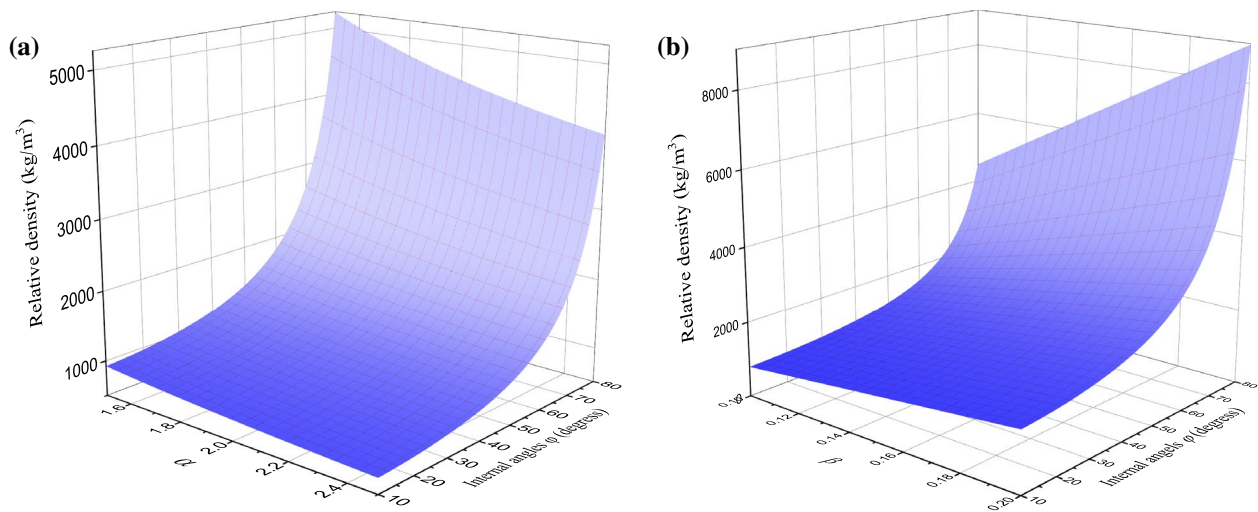
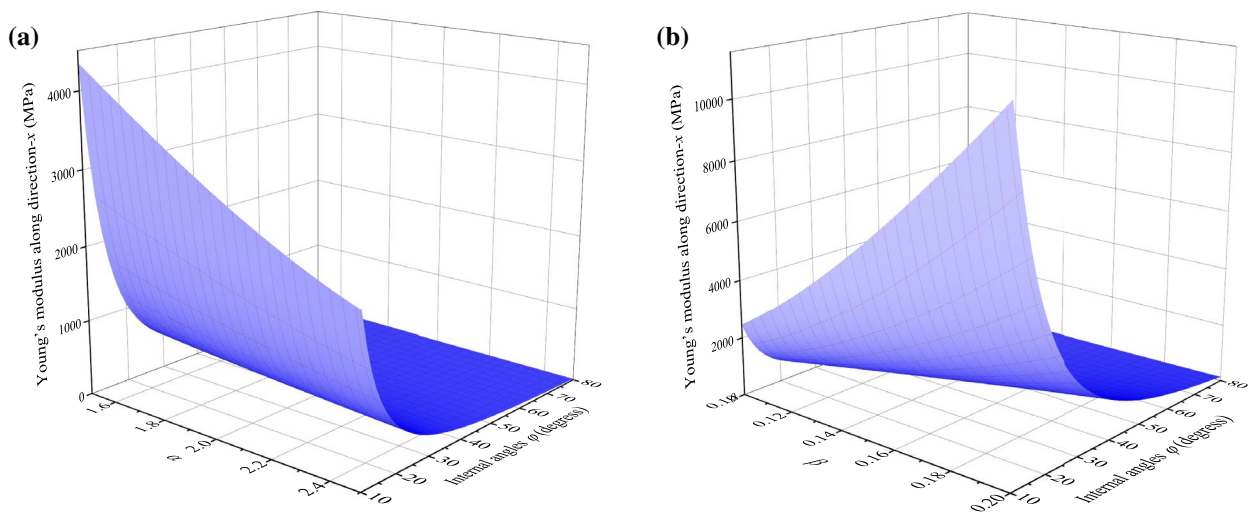**Fig. 9** Effect of **a** α and **b** β on the relative density of cellular core versus internal angle φ

Fig. 10 Effect of **a** α and **b** β on the elastic modulus in direction-x of cellular core versus φ

vibration characteristics of an isotropic cylindrical shell. In this case, the geometry dimensions and material properties are chosen as $E = 68.2$ GPa, $\rho = 2700$ kg/m^3, and $v = 0.33$. $L = 1.7272$ m, $R = 0.0762$ m, and $h = 0.00147$ m. In addition, unlike FEM analysis of effective mechanical properties, a 3D model with 8-node linear brick C3D8R is employed to calculate the natural frequencies of the elastic and isotropic cylindrical shell, as shown in Fig. 7. The boundary conditions are listed in Table 5, where u_i and UR_i are displacements in x, θ, and z directions and related rotations, respectively.

Figure 8 shows the errors for natural frequencies of the SS-SS shell obtained by experiment, Soedel, Flügge, Morley-Koiter, Donnell, and FEM relative to those obtained by the current method. It can be seen that some discrepancies

are made between the natural frequencies obtained by the present method and DST (Exact). Except for DST (Exact) and MKST (Exact), the error values of the natural frequencies of the SS-SS shell are less than 5%. Uncertainties affecting the results among those theories are due to the various assumptions made about the form of small terms and the order of terms that are retained in the analysis [41, 42]. Generally, the DST is the simplest of these theories. The FST is felt to be the most accurate. The various shell theories sometimes predict significantly different results [43]. However, over broad ranges of parameters of engineering importance, these theories yield similar results [44]. In addition, as shown in Table 4, the theoretical result of natural frequency in the current method is higher than the FEM and FST owing to the neglect of rotary inertia and shear deformation.
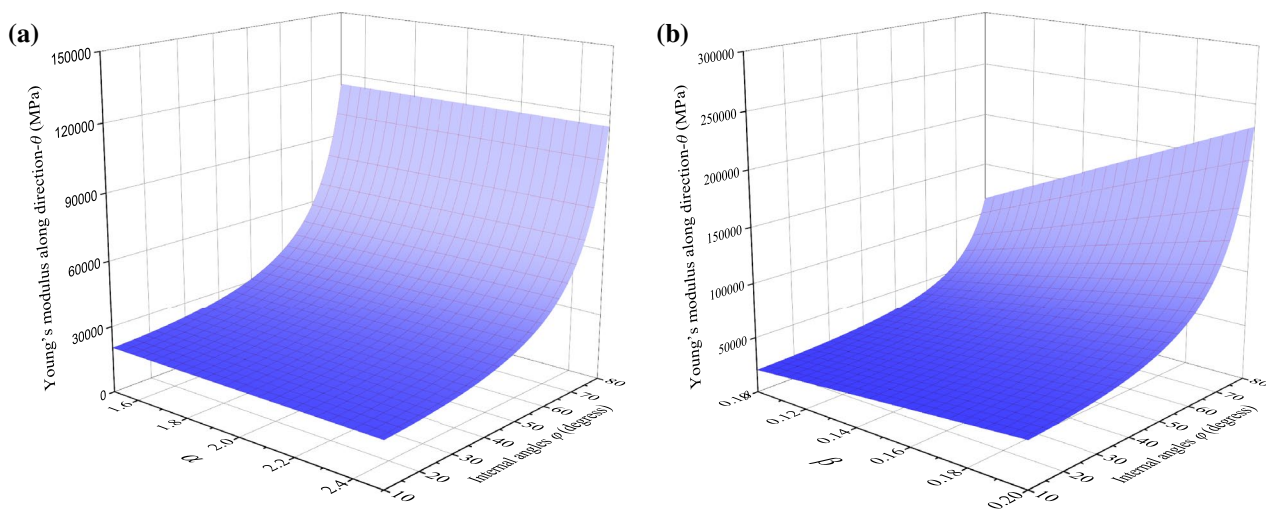
Fig. 11 Effect of **a** α and **b** β on the elastic modulus along direction-θ of cellular core versus φ

Results and Discussion

The structural parameter analysis is evaluated in this section. Since the validity of theoretical predictions is confirmed in FEM and some available literature results in Sect. "Numerical simulation", all the results are theoretical values according to Table 6 except those mentioned in this section.

Effective Mechanical Properties of ZPR Cellular Core Layer

Figure 9 describes the effects of α and β on the relative density of cellular core versus internal angle φ. The plot illustrates that an increased internal angle φ leads to an increase in the relative density of the cellular core when other parameters are given fixed values. In addition, geometric parameters, including α and β, provide opposite contributions to the relative density. In other words, a decrease of α and/or an increase of β will increase the cellular core's relative density when φ keeps constant. Indeed, the increase of φ can decrease the equivalent area of the cellular core, resulting in an increase in the relative density. While the equivalent area increases with decrease of α.

Figure 10 illustrates the effects of α and β on the elastic modulus along direction-x of cellular core versus φ. It is clear that the elastic modulus in direction-x decreases with increasing φ value for fixed α and β values, which is similar to Fig. 6(a). An increase of φ value leads to the increase of the bending of the cell wall along direction-x. Consequently, φ value is increased, resulting in a decreased elastic modulus in direction-x. From Fig. 10(a), it can be seen that the elastic modulus in direction-x decreases with the increase of α values when other parameters are given fixed values owing to the increased cross-sectional area induced by the parameters α. In

addition, Fig. 10(b) indicates that β increases, the elastic modulus in direction-x increases when other parameters are given fixed values. In the unit cell, increasing value of φ and decreasing value of β tend to increase the bending deformation along the direction-x, resulting in larger effective strains and lower equivalent elastic modulus. The decreasing value of α leads to smaller sectional area normal to loading direction, leading to large equivalent stress and elastic modulus in direction-x.

Figure 11 illustrates the effects of α and β on the elastic modulus along the direction-θ of the cellular core versus φ. The elastic modulus in direction-θ increases with the increase of φ value for fixed α and β values, which is similar to Fig. 6(b). An increasing internal angle φ decreases a cross-section perpendicular to the loading direction, leading to larger equivalent stress and elastic modulus. As shown in Fig. 11(a), the α value variations do not affect the elastic modulus in direction-θ when other parameters remain constant. According to the above analysis in Sect. 2.1, the deformations of diagonal and vertical walls have relative independence. No deformation occurs in sloping walls when the cellular structure suffers a tensile loading along the direction-θ. Therefore, the variations of α value are irrelevant to the elastic modulus in direction-θ. In addition, Fig. 11(b) indicates that an increase of β value leads to an increasing elastic modulus in direction-θ when other parameters remain constant owing to the increasing cross-section of vertical walls.

Natural Frequencies of Sandwich Cylindrical Shell

Figure 12 shows the effects of α on natural frequencies of the shell containing ZPR cellular core versus φ under different boundaries, where $\beta = 0.1$, $R = 0.2$ m, $h_0/h = 0.8$, $L/R = 5$, $R/h = 20$. The detailed values of natural frequency in Fig. 12
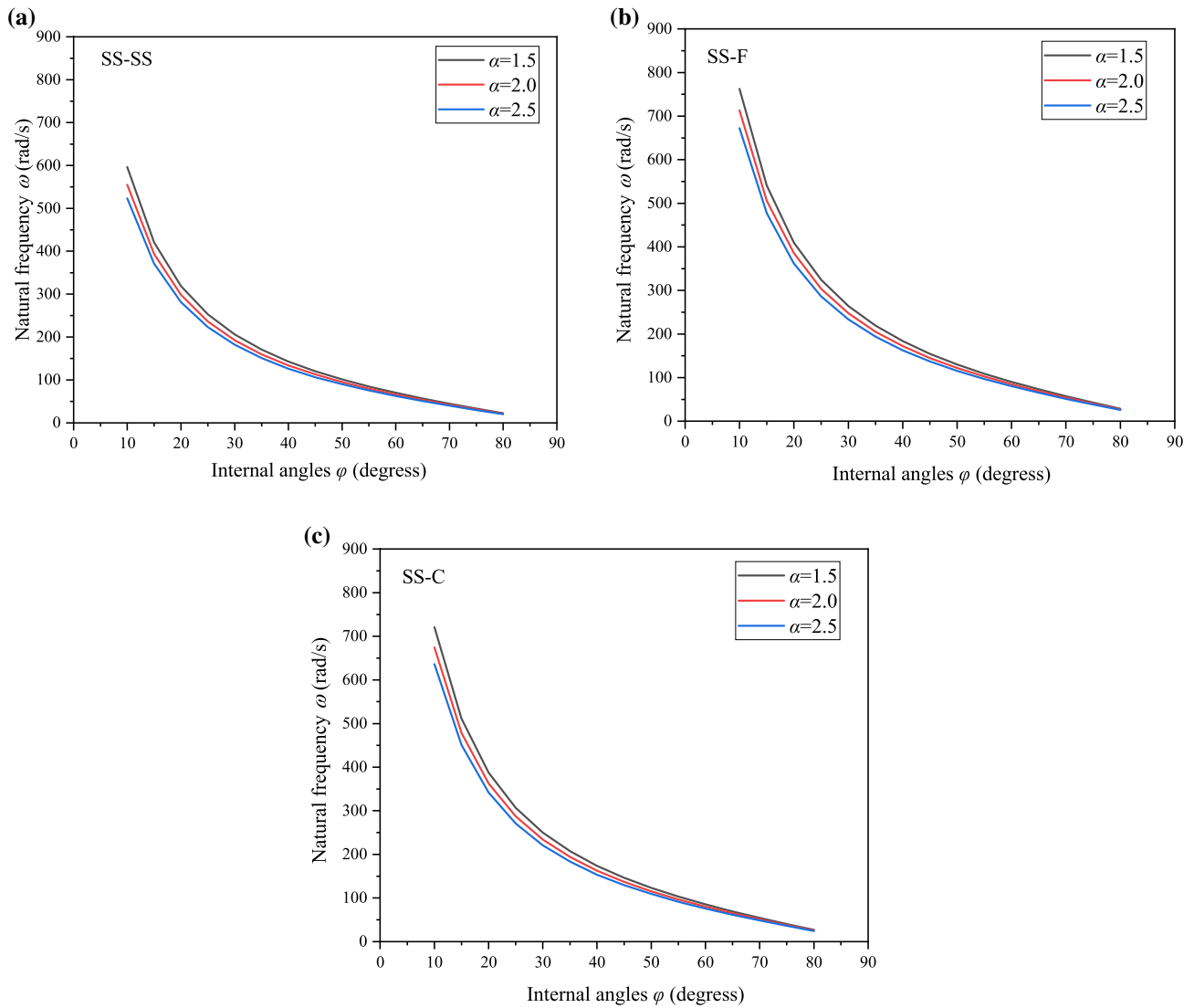
(a)

(b)

(c)

Fig. 12 Natural frequencies of the shell versus internal angles φ, for different α ($\beta=0.1$, $R=0.2$ m, $h_0/h=0.8$, $L/R=5$, $R/h=20$)

Table 7 Effects of α on natural frequencies of the shell containing ZPR cellular core versus φ under different boundaries ($\beta=0.1$, $R=0.2$ m, $h_0/h=0.8$, $L/R=5$, $R/h=20$)

| φ (degress)	SS-SS (rad/s)			SS-F (rad/s)			SS-C (rad/s)		
	$\alpha=1.5$	$\alpha=2.0$	$\alpha=2.5$	$\alpha=1.5$	$\alpha=2.0$	$\alpha=2.5$	$\alpha=1.5$	$\alpha=2.0$	$\alpha=2.5$
10	596.3	555.1	523.4	762.6	713.4	672.7	721.2	674.7	636.2
20	318.9	298.4	281.4	409.9	385.5	361.7	387.6	362.7	342.1
30	205.7	192.6	181.7	264.4	247.5	233.5	250.0	234.1	220.9
40	142.9	133.9	126.4	183.7	172.1	162.5	173.7	162.8	153.7
50	101.3	95.0	89.8	130.2	122.1	115.4	123.1	115.5	109.1
60	70.2	65.9	62.4	90.2	84.7	80.2	85.3	80.1	75.8
70	44.7	42.1	39.9	57.4	54.1	51.3	54.3	51.1	48.5
80	22.2	21.0	20.1	28.5	27.0	25.8	26.9	25.5	24.4
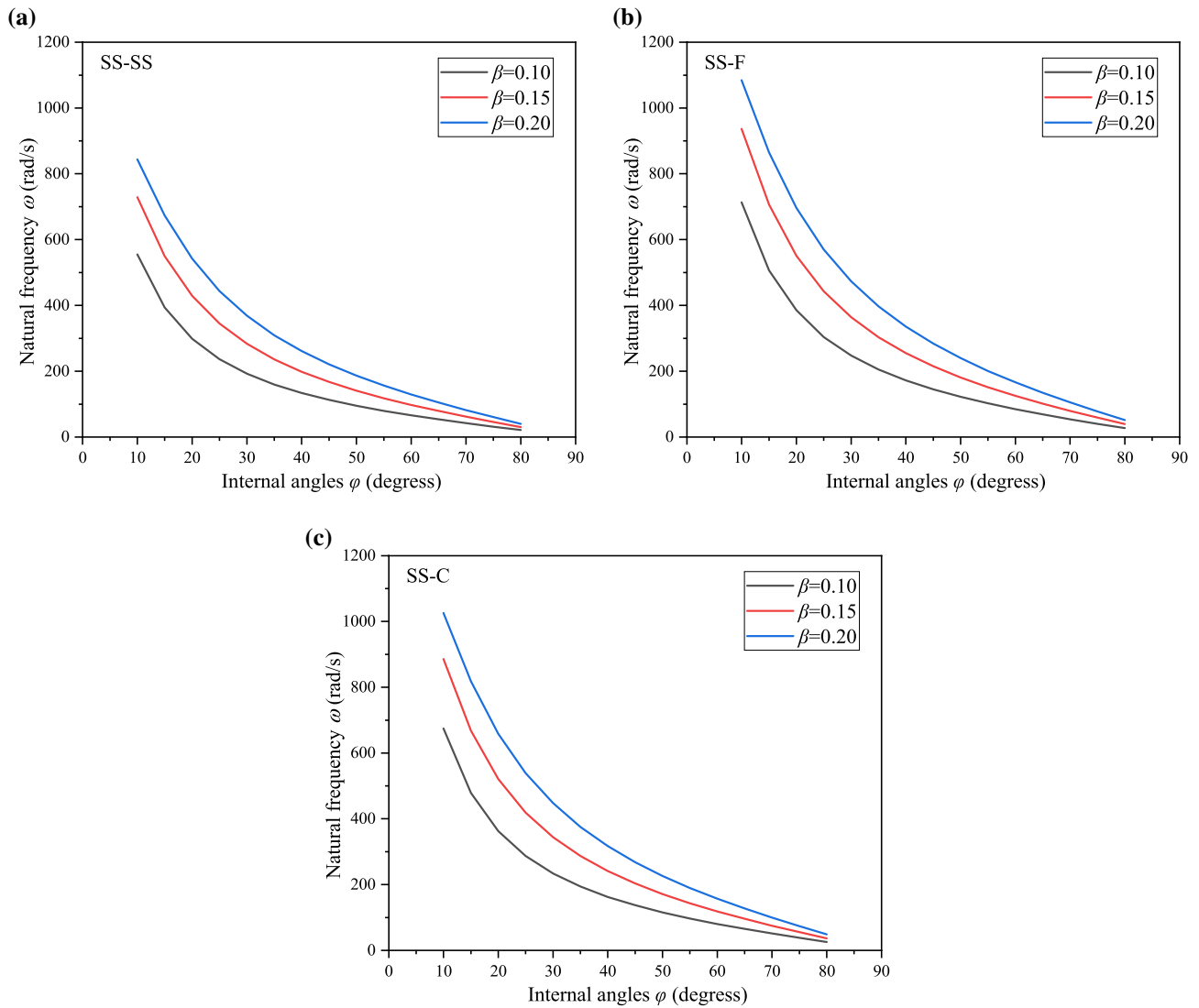
Fig. 13 Natural frequencies of the shell versus internal angles φ, for different β ($\alpha=2$, $R=0.2$ m, $h_0/h=0.8$, $L/R=5$, $R/h=20$)

Table 8 Effects of β on natural frequencies of the shell containing ZPR cellular core versus φ under different boundaries ($\alpha=2$, $R=0.2$ m, $h_0/h=0.8$, $L/R=5$, $R/h=20$)

φ (degress)	SS-SS (rad/s)			SS-F (rad/s)			SS-C (rad/s)		
	$\beta=0.10$	$\beta=0.15$	$\beta=0.20$	$\beta=0.10$	$\beta=0.15$	$\beta=0.20$	$\beta=0.10$	$\beta=0.15$	$\beta=0.20$
10	555.1	728.9	843.8	713.4	936.8	1084.5	674.7	886.0	1025.6
20	298.4	428.8	541.8	385.5	551.1	696.3	362.7	521.2	658.6
30	192.6	283.1	368.3	247.5	363.9	473.4	234.1	344.1	447.7
40	133.9	198.3	261.0	172.1	254.8	335.4	162.8	241.0	317.2
50	95.0	140.9	186.4	122.1	181.1	239.6	115.5	171.3	226.6
60	65.9	97.5	129.3	84.7	125.3	166.2	80.1	118.5	157.2
70	42.1	61.8	82.0	54.1	79.5	105.3	51.1	75.2	99.6
80	21.0	30.3	39.9	27.0	38.9	51.3	25.5	36.8	48.6

(a)

(b)

(c)
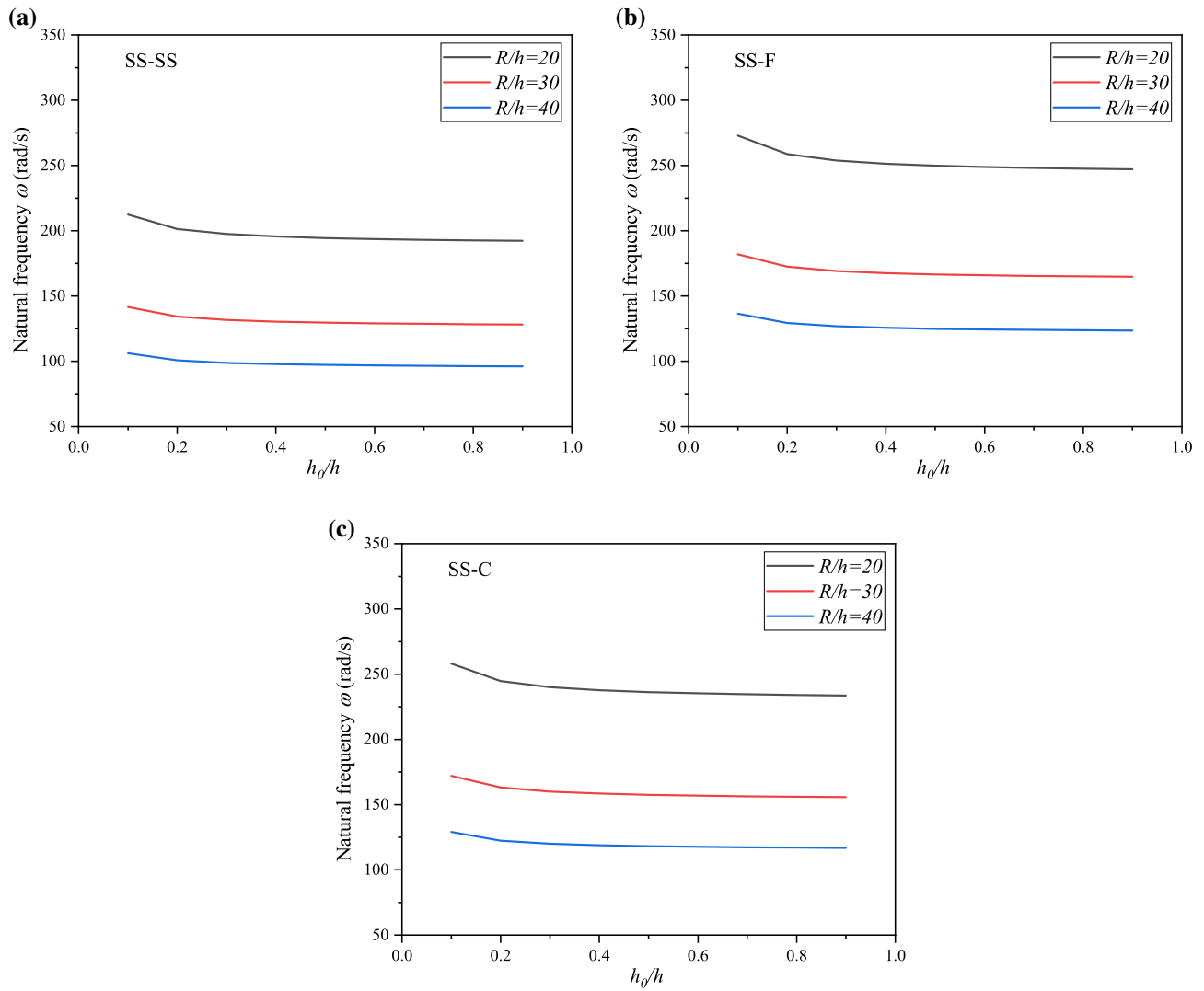
Fig. 14 Natural frequencies of the shell versus h_0/h for different R/h ($\alpha = 2$, $\beta = 0.1$, $\varphi = 30°$, $h = 0.01$ m, $L/R = 5$)

Table 9 Effects of R/h on natural frequencies of the shell containing ZPR cellular core versus h_0/h under different boundaries ($\alpha = 2$, $\beta = 0.1$, $\varphi = 30°$, $h = 0.01$ m, $L/R = 5$)

| h_0/h	SS-SS (*rad/s*)			SS-F (*rad/s*)			SS-C (*rad/s*)		
	$R/h = 20$	$R/h = 30$	$R/h = 40$	$R/h = 20$	$R/h = 30$	$R/h = 40$	$R/h = 20$	$R/h = 30$	$R/h = 40$
0.1	212.4	141.6	106.2	272.9	182.0	136.5	258.1	172.1	129.1
0.2	201.3	134.2	100.7	258.8	172.5	129.6	244.7	163.2	122.4
0.3	197.5	131.7	98.8	253.8	169.2	126.9	240.1	160.0	120.0
0.4	195.6	130.4	97.8	251.3	167.6	125.7	237.7	158.5	118.8
0.5	194.4	129.6	97.2	249.8	166.5	124.9	236.3	157.5	118.1
0.6	193.6	129.0	96.8	248.8	165.9	124.4	235.3	156.9	117.6
0.7	193.0	128.7	96.5	248.1	165.4	124.0	234.6	156.4	117.3
0.8	192.6	128.4	96.3	247.5	165.0	123.8	234.1	156.1	117.0
0.9	192.2	128.2	96.1	247.1	164.7	125.5	233.7	155.8	116.8
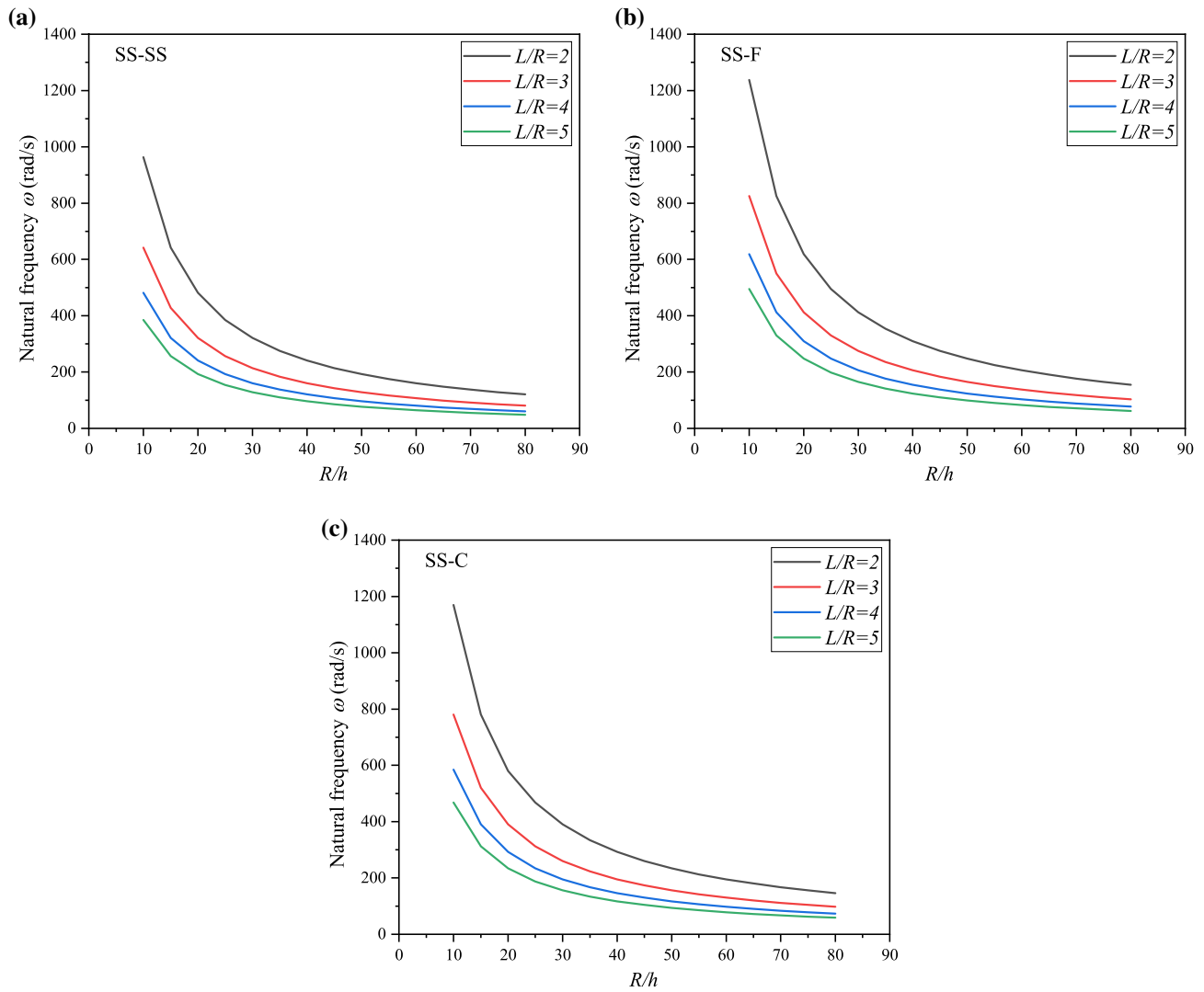
Fig.15 Natural frequencies of the shell versus *R/h* for different *L/R* ($\alpha=2$, $\beta=0.1$, $\varphi=30°$, $h=0.01$ m, $h_0/h=0.8$)

Table 10 Effects of *L/R* on natural frequencies of the shell containing ZPR cellular core versus *R/h* under different boundaries ($\alpha=2$, $\beta=0.1$, $\varphi=30°$, $h=0.01$ m, $h_0/h=0.8$)

R/h	SS-SS (*rad/s*)				SS-F (*rad/s*)				SS-C (*rad/s*)			
	L/R=2	*L/R*=3	*L/R*=4	*L/R*=5	*L/R*=2	*L/R*=3	*L/R*=4	*L/R*=5	*L/R*=2	*L/R*=3	*L/R*=4	*L/R*=5
10	962.9	641.9	481.4	385.2	1237.5	825.0	618.8	495.0	1170.4	780.3	585.2	468.2
20	201.3	321.0	240.7	192.6	618.8	412.5	309.4	247.5	580.2	390.1	292.6	234.1
30	197.5	214.0	160.5	128.4	412.5	275.0	206.3	165.0	390.1	260.1	195.1	156.1
40	195.6	160.5	120.4	96.3	309.4	206.3	154.7	123.8	292.6	195.1	146.3	117.0
50	194.4	128.4	96.3	77.0	247.5	165.0	123.8	99.0	234.1	156.1	117.0	93.6
60	193.6	107.0	80.2	64.2	206.3	137.5	103.1	82.5	195.1	130.0	97.5	78.0
70	193.0	91.7	68.8	55.0	176.8	117.9	88.4	70.7	167.2	111.5	83.6	66.9
80	192.6	80.2	60.2	48.1	154.7	103.1	77.3	61.9	146.3	97.5	73.1	58.5

are listed in Table 7. It can be concluded that the natural frequencies of this system decrease with the increase of φ value for SS-SS, SS-F, and SS-C boundary conditions. In addition, an increase of α results in decline in natural frequencies.

Figure 13 exhibits the effects of β on natural frequencies of the shell containing ZPR cellular core versus φ under different boundaries, where $\alpha = 2$, $R = 0.2$ m, $h_0/h = 0.8$, $L/R = 5$, $R/h = 20$. Natural frequencies of this system increase with the increase of β value. The detailed values of natural frequency in Fig. 13 are listed in Table 8. From the mechanical properties of the cellular core obtained in Sect. "Effective Mechanical properties of ZPR Cellular Core Layer", we can conclude that an increasing internal angle φ leads to an increase in the relative density, resulting in lower natural frequencies. Likewise, the intricate trend of natural frequencies induced by α and β can be expounded by the mechanical properties of the cellular core. As shown in Fig. 9, an increase of α and/or a decrease of β will increase the overall mass, resulting in the natural frequencies decreasing.

Figure 14 shows the effects of radius-to-thickness ratio R/h on natural frequencies of the shell versus containing ZPR cellular core core-thickness ratio h_0/h under different boundaries, where $\alpha = 2$, $\beta = 0.1$, $\varphi = 30°$, $h = 0.01$ m, $L/R = 5$. The detailed values of natural frequency in Fig. 14 are listed in Table 9. Results show that as R/h increases, the natural frequencies decrease. Moreover, the natural frequencies decrease with the increase of h_0/h. That is, the density of elastic and isotropic materials is less than that of this system's cellular core. When the shell thickness h is given a definite value, an increase in core thickness h_0 leads to the reduction of the inner and outer layer thickness. In other words, the increased h_0 will increase the shell's overall mass, resulting in the natural frequencies decreasing. In addition, the increased h_0 can weaken the core layer's enhancement effect on the sandwich shell's global bending rigidity, leading to the decline of the global bending rigidity of the sandwich shell. At this point, the enhancement effect of the core layer as the upper and lower panel spacing on the overall bending stiffness of the sandwich shell is weakened, resulting in the reduction of the overall bending stiffness of the sandwich shell.

Figure 15 shows the influences of length-to-radius ratio L/R on natural frequencies of the shell containing ZPR cellular core versus R/h under different boundary conditions, where $\alpha = 2$, $\beta = 0.1$, $\varphi = 30°$, $h = 0.01$ m, $h_0/h = 0.8$. The detailed values of natural frequency in Fig. 15 are listed in Table 10. Those diagrams illustrate the natural frequencies decrease with the increase of the L/R, which is very similar to what was reported by Li et al. [45]. This intuitively correct because the stiffness decreases with the increases in length.

Conclusions

This work investigates the effective mechanical properties of a ZPR cellular core and the vibrational behavior of sandwich cylindrical shells with the ZPR cellular core. Homogenization methods are used to analyze the effective mechanical properties of the cellular core. The CLST and Hamilton principles are employed to form the equilibrium equations to determine the vibrational behavior of the sandwich cylindrical shells. The small discrepancies between the theoretical predictions and the FEM results prove the analytical models are accurate for engineers to quickly select geometric parameters in designing a desired structure. The following conclusions are drawn from this study:

(1) These structural geometric parameters contribute to the effective mechanical performances of the ZPR cellular core, including the relative density and the effective modulus. For example, an increased α and/or a decreased β will lead to the relative density of the cellular core increasing, and the elastic modulus in direction-x of the cellular core decreases with the increase of α while increases with the increase of β.

(2) The effective mechanical performances of the cellular core and geometric parameters of the shell can influence the natural frequencies of the sandwich cylindrical shell under different boundaries driven by changing overall mass and bending rigidity of the sandwich shell. For example, an increase of α and/or a decrease in β leads to an increase in relative density, resulting in larger natural frequencies. The increase of core thickness h_0 leads to the natural frequencies decrease owing to the weakened overall bending rigidity of the sandwich shell.

Declarations

this study are available upon request by contact with the corresponding author.

References

1. Ren F, Liu H (2022) Strain induced low frequency broad band-gap tuning of the multiple re-entrant star shaped honeycomb with negative poisson's ratio. J Vib Eng Technol. https://doi.org/10.1007/s42417-022-00547-3

2. Zhang J, Dong B, Zhang W (2021) Dynamic crushing of gradient auxetic honeycombs. J Vib Eng Technol 9:421–431. https://doi.org/10.1007/s42417-020-00236-z

3. Chang LL, Shen X, Dai YK, Wang TX, Zhang L (2020) Investigation on the mechanical properties of topologically optimized cellular structures for sandwiched morphing skins. Compos Str 250:112555. https://doi.org/10.1016/j.compstruct.2020.112555

4. Vaishali KS, Kumar RR, Dey S (2022) Sensitivity analysis of random frequency responses of hybrid multi-functionally graded sandwich shells. J Vib Eng Technol. https://doi.org/10.1007/s42417-022-00612-x

5. Khaire N, Tiwari G, Rathod S, Iqbal MA, Topa A (2022) Perforation and energy dissipation behaviour of honeycomb core cylindrical sandwich shell subjected to conical shape projectile at high velocity impact. Thin-Walled Str 171:108724. https://doi.org/10.1016/j.tws.2021.108724

6. Song L, Yin Z, Wang T, Shen X, Wu J, Su M, Wang HJ (2021) Nonlinear mechanics of a thin-walled honeycomb with zero Poisson's ratio. Mech Based Des Str Mech. https://doi.org/10.1080/15397734.2021.1987262

7. Qiu C, Guan Z, Jiang S, Li Z (2017) A method of determining effect elastic properties of honeycomb cores based on equal strain energy. Chin J Aeronaut 30:766–799. https://doi.org/10.1016/j.cja.2017.02.016

8. Dai G, Zhang W (2009) Cell size effect analysis of the effective Young's modulus of sandwich core. Comput Mater Sci 46:744–748. https://doi.org/10.1016/j.commatsci.2009.04.033

9. Yazdanparast R, Rafiee R (2022) Developing a homogenization approach for estimation of in-plan effective elastic moduli of hexagonal honeycombs. Eng Anal Bound Elem 117:202–211. https://doi.org/10.1016/j.enganabound.2020.04.012

10. Gonella S, Ruzzene M (2008) Homogenization and equivalent in-plane properties of two-dimensional periodic lattices. Int J Solids Str 45:1897–1915. https://doi.org/10.1016/j.ijsolstr.2008.01.002

11. Gibson LJ, Ashby MF, Schajer GS, Robertson CI (1982) The mechanics of two-dimensional cellular materials. Proc R Soc Lond A 382:25–42. https://doi.org/10.1098/rspa.1982.0087

12. Olympio KR, Gandhi F (2010) Zero Poisson's ratio cellular honeycombs for flex skins undergoing one-dimensional morphing. J Intell Mater Syst Str 21:1737–1753. https://doi.org/10.1177/1045389X09355664

13. Yu XL, Zhou J, Liang HY, Jiang ZY (2018) Wu L L (2018) Mechaincal metamaterials associated with stiffness, rigidity and compressibility: A brief review. Prog Mater Sci 94:114–173. https://doi.org/10.1016/j.pmatsci.2017.12.003

14. Zhong R, Ren X, Zhang XY, Luo C, Zhang Y, Xie YM (2022) Mechanical properties of concrete composites with anxetic single and layered honeycomb structures. Constr Build Mater 322:126453. https://doi.org/10.1016/j.conbuildmat.2022.126453

15. Liu W, Li H, Zhang J, Li H (2018) Elastic properties of a novel cellular structure with trapezoidal beams. Aerosp Sci Technol 75:315–328. https://doi.org/10.1016/j.ast.2018.01.020

16. Gong X, Huang J, Scarpa F, Liu Y, Leng J (2015) Zero Poisson's ratio cellular structure for two-dimensional morphing application. Compos Str 134:384–392. https://doi.org/10.1016/j.compstruct.2015.08.048

17. Feng N, Tie YH, Wang SB, Guo JX, Hu ZG (2022) Mechanical performance of 3D-printing annular honeycomb with tailorable Poisson's ratio. Mech Adv Mater Str. https://doi.org/10.1080/15376494.2022.2083733

18. Tornabene F (2016) Gennral higher-order layer-wise theory for free vibrations of doubly-curved laminated composite shells and panels. Mech Adv Mater Str 23:1046–1067. https://doi.org/10.1080/15376494.2015.1121522

19. Huang J, Zhang Q, Scarpa F, Liu Y, Leng J (2016) Bending and benchmark of zero Poisson's ratio cellular structures. Compos Struct 152:729–736. https://doi.org/10.1016/j.compstruct.2016.05.078

20. Neville RM, Mobti A, Hazra K, Scarpa F, Remillat C, Farrow IR (2014) Transverse stiffness and strength of Kirigami zero-v PEEK honeycombs. Compos Struct 114:30–40. https://doi.org/10.1016/j.compstruct.2014.04.001

21. Reissner E (1945) The effect of transverse shear deformation on the bending of elastic plates. J Appl Mech-Trans ASME 12:68–77. https://doi.org/10.1115/1.4009435

22. Reddy JN (1984) A simple Higher-order theory for laminated composite plates. J Appl Mech-Trans ASME 51:745–752. https://doi.org/10.1115/1.3167719

23. Wang P, Chalal H, Abed-Meraim A (2017) Quadratic prismatic and hexahedral solid-shell elements for geometric nonlinear analysis of laminated composite structures. Compos Str 172:280–296. https://doi.org/10.1016/j.compstruct.2017.03.091

24. Duc ND, Thang PT (2015) Nonlinear response of inperfect eccentrically stiffened ceramic-metal-ceramic Sigmoid Functionally Graded Material (S-FGM) thin circular cylindrical shells surrounded on elastic foundations under uniform radial load. Mech Adv Mater Str 22:1031–1038. https://doi.org/10.1016/j.compstruct.2013.11.015

25. Qin ZY, Pang XJ, Safaei B, Chu FL (2019) Free vibration analysis of rotating functionally graded CNT reinforced composite cylindrical shells with arbitray boundary conditions. Compos Str 220:847–860. https://doi.org/10.1016/j.compstruct.2019.04.06

26. Pang FZ, Li HC, Chen HL, Shan YH (2021) Free vibration analysis of combined composite laminated cylindrical and spherical shells with arbitray boundary conditions. Mech Adv Mater Str 28:182–199. https://doi.org/10.1080/15376494.2018.1553258

27. Eipakchi H, Nasrekani FM (2020) Vibrational behavior of composite cylindrical shells with auxetic honeycombs core layer subjected to a moving pressure. Compos Struct 254:112847. https://doi.org/10.1016/j.compstruct.2020.112847

28. Lan L, Sun J, Hong F, Wang D, Zhang Y, Fu M (2020) Nonlinear constitutive relations of thin-walled honeycomb structure. Mech Mater 149:103556. https://doi.org/10.1016/j.mechmat.2020.103556

29. Gibson LJ, Ashby MF (1997) Cellular solid: structure and properties. Cambridge University Press

30. Young WC (2002) Cark's formulas for stress and strain. McGraw-Hill Education, New York https://doi.org/10.1115/1.3423917

31. Becus GA (2019) Homogenization and random evolutions: Applications to the mechanics of composite materials. Q appl Math 37:209–210. https://doi.org/10.1090/qam/548985

32. Hamidreza E, Nasrekani FM, Ahmadi S (2020) An analytical approach for vibration behavior of viscoelastic cylindrical shells under internal moving pressure. Acta Mech 231:3405–3418. https://doi.org/10.1007/s00707-020-02719-2

33. Sadd MH (2007) Elastic theory, application, and numeric. Academic Press

34. Pham HC, Pham TL, Nguyen VN, Nguyen DD (2019) Geometrically nonlinear dynamic response of eccentrically stiffened circular cylindrical shells with negativePoisson's ratio in auxetic honeycombs core layer. Int J Mech Sci 152:443–453. https://doi.org/10.1016/j.ijmecsci.2018.12.052

35. Rao SS (2007) Vibration of continuous system. New Jersey, USA: John Willey & Sons

36. Pradhan SC, Loy CT, Lam KY, Reddy JN (2000) Vibration characteristics of functionally graded cylindrical shells under various boundary conditions. Appl Acoust 61:111–129. https://doi.org/10.1016/S0003-682X(99)00063-8

37. Loy CT, Lam KY (1997) Vibration of cylindrical shells with ring support. Int J Mech Sci 39:455–471. https://doi.org/10.1016/S0020-7403(96)00035-5

38. Bubert EA, Woods BKS, Lee K, Kothera CS, Wereley NM (2010) Design and fabrication of a passive 1D morphing aircraft skin. J Int Mater Syst Struct 21:1699–1717. https://doi.org/10.1177/1045389X10378777

39. Farshidianfar A, Farshidianfar MH, Crocker MJ, Smith WO (2011) The vibration analysis of long cylindrical shells using acoustical excitation. J Sound Vibr 330:3381–3399. https://doi.org/10.1016/j.jsv.2011.02.002

40. Oliazadeh P, Farshidianfar MH, Farshidianfar A (2013) Exact analysis of resonance frequency and mode shapes of isotropic and laminated composite cylindrical shells; Part I: analytical studies. J Mech Sci Technol 27:3635–3643. https://doi.org/10.1007/s12206-013-0905-1

41. Flügge W (1973) Stresses in Shells. Second Springer, Berlin

42. Dinh GN, Nguyen DT, Vu NVH, Dao HB (2020) Vibration of cylindrical shells made of three layers W-Cu composite containing heavy water using Flügge-Lur'e-Bryrne theory. Thin-Walled Struct 146:106414. https://doi.org/10.1016/j.tws.2019.106414

43. Singal RK, Williams K (1988) A theoretical and experimental study of vibrations of thick circular cylindrical shells and rings. J Vib Acoust 110:533–537. https://doi.org/10.1115/1.3269562

44. Blevins RD (1987) Formulas for natural frequency and mode shape. Robert E. Krieger Publishing Co., FL

45. Li Y, Yao W, Wang T (2020) Free flexural vibration of thin-walled honeycomb sandwich cylindrical shells. Thin-walled Struct 157:107032. https://doi.org/10.1016/j.tws.2020.107032